Journal of Petroleum Exploration and Production Technology (2023) 13:1519–1534
https://doi.org/10.1007/s13202-023-01627-0

ORIGINAL PAPER-PRODUCTION ENGINEERING

Experimental simulation of wormhole sanding cavity pattern and microscopic mechanism in heterogeneous weakly-cemented sandstone

Yajun Song[1,2] · Changyin Dong[1,2] · Bo Zhou[1,2] · Xinjie Zhan[1,2] · Gerald Gwamba[2]

Received: 24 October 2022 / Accepted: 18 March 2023 / Published online: 1 April 2023

Abstract

Sand production has been a shared problem in the development of weakly-cemented sandstone oil reservoirs. Sanding simulation and prediction are of utmost importance for the production optimization of this type of reservoir. For a long time, research on sand production has been centered on "what is produced from the formation," such as the size and rate of produced sand. However, "what is left inside the formation," which is the structural change of the rock after sanding, is also another intriguing and important topic for the management of sand-prone reservoirs. Some related studies have been carried out, and they have proposed that wormhole-like pore throat will appear after sand production, but the precise morphological description and formation mechanism are still lacking. A series of sanding simulation experiments are performed to deepen the understanding of the sanding cavity pattern and its mechanism. The experiments are carried out using a visual sanding simulation apparatus. Through this, the complex wormhole sand production patterns are found and classified into single-branch wormhole cavity patterns and multi-branch wormhole cavity patterns. The extension processes of those different patterns are also demonstrated. Besides, this work discusses the change in the reservoir flowability performance in wormhole sanding mode, and the near-well flowability might be improved by actively inducing weakly-cemented sandstone to create a bigger aperture wormhole sanding pattern. Through the visual microscopic system, the sand competitive detachment mechanism that induces wormhole extending is revealed, along with the cavities concurrent extension mechanism that induces multi-branch wormhole extending. Moreover, this work discusses the microscopic detachment forms which help explain the sand-produced rate from weakly-cemented sandstone. This work enhances and creates a novel understanding of the sanding patterns and mechanisms in weakly-cemented heterogeneous reservoirs, which is beneficial to providing direct guidance for sand production prediction and sand control optimization.

Keywords Weakly-cemented sandstone · Sanding simulation experiment · Wormhole sanding cavity · Microscopic sanding mechanism · Sand production law

Abbreviations

MBW	Multi-branch wormhole
SBW	Single-branch wormhole
UCS	Uniaxial compressive strength
VSSA	Visual sanding simulation apparatus

List of symbols

$\overline{d_{\max}}$	Average maximum aperture (mm)
d_{ef}	Dredging efficiency (MPa mm/s)
ΔP	Pressure drop during water flooding (MPa)
T	Water flooding time (s)
V_{r}	Sanding cavity volume ratio (%)

Introduction

A major current focus on weakly-cemented sandstone reservoir production is how to control sand grain migration. An effective forecast of sand production can serve as a strategic foundation for ensuing sand control. Additionally, the simulation of the sanding cavity in the weakly-cemented reservoir

✉ Changyin Dong
dongcy@upc.edu.cn

[1] Key Laboratory of Unconventional Oil & Gas Development (China University of Petroleum (East China)), Ministry of Education, Qingdao 266580, Shandong, China

[2] School of Petroleum Engineering, China University of Petroleum (East China), Qingdao 266580, Shandong, China

and the microscopic sand particle migration law are crucial for sand production prediction. Over the past decades, the sanding prediction numerical simulation and sand particle release law of weakly-cemented sandstone reservoirs have been the extensive research subjects, which have led to the relatively systematic foundation of theory and methodology. For decades, researchers mostly developed sand production prediction models based on the Mohr–Coulomb criterion, which suggested that sand transportation originated from the formation rock shear and tension failure (El-Sayed and Alsughayer 2001; Morita 1994; Alireza Nouri et al. 2007; Volonté et al. 2013; Wang and Zhang 2002; Wei et al. 2011; Weingarten and Perkins 1995). The analysis method based on the theory is relatively conservative, and in fact, many oilfield wells do not produce sand even under the predicted critical conditions (Weingarten and Perkins 1995). It is considered that sand production consists of two essential processes: rock failure and hydrodynamic transport to the wellbore of sandstone particles. Perforations can further complicate the effective stress patterns around the wellbore which may worsen the problem (Alireza Nouri et al. 2003). Meanwhile, some research also took the ductile failure of the weakly-cemented sandstone into consideration proposing that the reservoir stratum will suddenly break down and produce sand when the plastic deformation exceeds the limiting strain value and successively established prediction models for sand production from weakly-cemented sandstone reservoirs (Nouri et al. 2009; Polillo et al. 1994; Wang and Sharma 2018). Macro-static factors and dynamic factors can reduce the strength of weakly-cemented sandstone and thus indirectly induce grains released from the formation. The sand production prediction model that varies with the production period was designed to calculate the critical drawdown under different water-bearing saturation states (Du et al. 2009). The above sand production mechanism and prediction methods are mainly based on the rock damage criterion from the macroscopic perspective. Moreover, existing sand production mechanism and prediction methods hardly explain and describe the microscopic particle detachment and transportation phenomena, especially the actual sand production rate and sand production pattern of the non-homogeneous oil fields.

On the other hand, some scholars have examined the microscopic sand production method and pattern of weakly-cemented sandstone and discovered that fluids mostly affect the loose sand particles by wrapping and transporting them rather than by mechanically harming the rock itself (Bagrezaie et al. 2022; Dong et al. 2020; Han et al. 2020; Russell et al. 2017; van den Hoek et al. 2000). Afterward, the mechanism of sand detachment from the rock skeletons and sand transportation was developed (Gwamba et al. 2022; Hashemi et al. 2022). The results of sand production experiments in large cavities showed that the main role of fluid flow in sanding is to carry the particles and grains generated by compression failure to the rock rather than damage the formation rock itself (van den Hoek et al. 2000). Particle migration in weakly-cemented sandstone aggravates formation inhomogeneity, resulting in lower ultimate oil recovery than normally consolidated sandstones (Ju et al. 2006). A conceptual model of particle release, suspension, and capture was put forth to study the transit of clay inside rocks (Khilar and Fogler 1983). Several particles transport plugging models and experiments have been run based on the Khilar model to investigate the porosity and permeability variations brought on by sand migrations as well as the distribution of residual oil (Habibi et al. 2012; Prempeh et al. 2020; You et al. 2013). Researchers have combined the erosion model with the stress model by volume strain based on the deformation of the oil sand matrix and discovered that a "wormhole" might form along the direction of the maximal permeability and porosity due to the presence of reservoir inhomogeneity (Wan and Wang 2004). It was proposed that the degree of particle migration is mainly influenced by fluid flow rate variation that is greater than the flow rate itself. Large pores are more likely to occur in reservoirs with weak cementation and high permeability, which provided early theoretical support for particle migration and sand production patterns (You et al. 2004; Zeng et al. 2005). The microscopic spalling and transporting behavior might cause changes in the rock skeleton construction and the formation of deficit macropores, which greatly impact the physical properties such as the permeability of the formation (Bagrezaie et al. 2022; Han et al. 2020; Russell et al. 2017). For inhomogeneous reservoirs and formations ranging in different cementation strengths, some researchers have initially proposed sand production patterns of pore liquefaction, wormhole, and continuous cavity, through visualizing sand production experiments, which have improved the understanding of sand particle migration mechanism from the microscopic perspective (Dong et al. 2020). The experiments revealed the wormhole pattern produced by the sand intrusion in the gravel layer of high mud-bearing strata, which further verified the universality of the wormhole sand production pattern and inspires the research of the sanding mechanism and pattern (Dong et al. 2022; Jin et al. 2021).

Overall, these studies of sand production mechanism and sand prediction have enriched and advanced the understanding of solid-phase production. The limitations are that the studies of sand migration mechanism are currently focused on macroscopic mechanical rock failure, and the understanding of the microcosmic mechanism and sanding cavity pattern extension law for various strength non-homogeneous reservoirs is not deep and systematic enough. It is also difficult to simulate and predict the structural changes of near-well reservoirs, especially the cavity pattern left after sand peeling off and transporting. In response to the above

problems, experiments were conducted on the sand production pattern and mechanism of this type of reservoir to reveal the complex sanding cavity, analyzing its extensional mechanism. Meanwhile, the flowability performance is studied to better know how the wormhole sanding pattern impact on the near-well reservoirs. The authors conduct a targeted study of wormhole sanding patterns, clearly presenting various wormhole results and their extending progress in the weakly-cemented sandstone reservoir, quantitatively analyzing the effect on reservoir flowability performance, which is different from the previous research. Moreover, this work innovatively studies the generation and extension mechanism of wormhole cavity patterns by capturing the behavior of micro-sand grains while flooding and reveals the basic cause of multi-branch wormhole pattern generation.

This work first introduces the experiment methods. Then, this work displays the main experimental results of macroscopic sand production patterns. And later this work establishes a quantitative method to compare various sand production patterns and discusses how those patterns affect the oil reservoir. Thirdly, it discusses the extending mechanism and microscopic detachment behavior of the sand production wormhole patterns. The analysis of wormhole and microscopic mechanism could be used to explain the macroscopic sand production problem in the oil field. Finally, the important conclusions are organized at the end of this paper.

Experiment methods

Experiment apparatus

The study relies on the micro-visualization sand production simulation experiments through the visual sanding simulation apparatus (abbreviated as VSSA), as shown in Fig. 1. The VSSA is a small-scale fluid-driven sand production simulation system. It is equipped with a high-pressure plunger pump which provides up to 15-MPa fluid pressure. The system is mainly designed to observe and capture the sand production process and mechanism induced by stress and fluid at the granular scale. Furthermore, the system can be used to study the transporting and clogging phenomena of sand particles in porous media by microscopic observation. The VSSA system is computer-controlled and consists of the following main parts: sanding simulation models, a high-pressure plunger pump, a microscopic observation module, a sand collector, pressure sensors, and a data acquisition system (Fig. 2). The pipeline connecting the high-pressure plunger pump to the injection side of the sanding simulation models serves as the system's power source. It can provide up to 600-mL/min fluid flow rate with an accuracy of ± 0.5%. The microscopic observation module primarily consists of a video microscope with 50–400 times magnification (refer

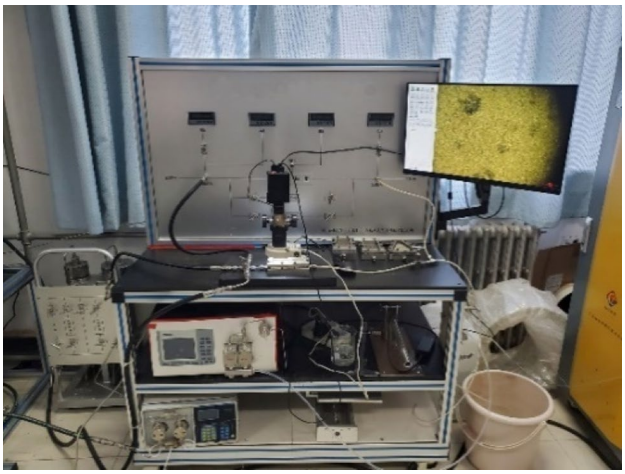

Fig. 1 General view of the visualization system for the microscopic process of sand production

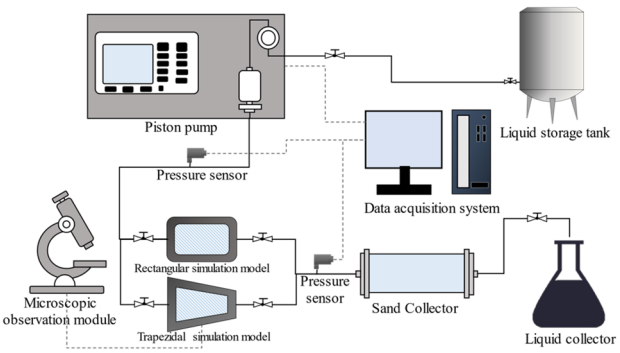

Fig. 2 Schematic of the visualization system for the microscopic process of sand production

to 20" monitor), which is mainly used for timely observation, photography, and video recording of visual sandstone models during experiments. There are two pressure sensors: one is installed at the injection side of the thin section sandstone models with a measuring range of 15 MPa, and the other is installed at the outflow side with a measuring range of 0.6 MPa. The measurement accuracy of both the inlet and outlet pressure is 0.1%, and it is accompanied by a power supply, conversion module, and data acquisition software. The output sand–water mixture from the thin section of the sandstone model will be separated through the sand collector, discharging the waste liquid into the liquid collector. The sand collector volume is up to 50 g, while 3-L liquid can be held in the liquid collector, allowing for uninterrupted continuous experiments. The produced sand in the sand collector is dried and weighed to obtain the final sand production rate after the experiment. A total of 6-mm piping and valves are employed in the whole VSSA system. The data acquisition system is connected to the pressure

sensors and the plunger pump to directly read and record the injection pressure, outlet pressure, and flow rate during the experiment. Thus, the pressure drops and flow variation patterns in complex sand production modes can be analyzed.

Main sanding simulation models

The trapezoidal sanding models and the rectangular sanding models are designed, respectively (Fig. 3), to simulate near-well stratigraphy characteristics and far-well stratigraphy characteristics, which are the key parts of the VSSA. Since it is difficult to fetch thin sections of rock from weakly-cemented sandstone formations, the modes are designed and used to contain the simulation sanding sample. Each of them can be considered a stratigraphic unit. To ensure the sanding takes place at the surface of samples and to visually observe the sanding cavity with its extending process, the thin models must be designed carefully with a sand-filling thickness of 5 mm, together with a transparent cover for taking pictures. The trapezoidal model is 16-mm wide at the top base, 80-mm wide at the bottom base, and 100-mm long, with a sand-filling volume of 45 g. The rectangular model is 50-mm wide and 100-mm long, with a sand-filling volume of 47 g. Both of the models are designed with a thin sand-filling thickness of 5 mm to visualize the process of carving the sandstone skeleton by the sand particle migration on a two-dimensional plane. The main purpose of this work is to observe the extending cavity caused by sand production. And the characteristics of the sanding cavities are mainly dominated by cementing strength along with its non-homogeneous and stochastic distribution. Due to the poor pressure resistance of the thin models, extra confining stress was not applied in this experiment to achieve the main purpose. The trapezoidal model was mainly used, which itself generates a certain amount of confining stress when a high fluid pressure gradient and flow rate are applied because of the gradually narrowing shape. Further study on this topic will be continually conducted in the future and will take confining stress as an important factor into consideration. The fluid is injected from the wider end of the trapezoidal sandstone model, converges at the narrow end, and then flows out (Fig. 3a). The convergence phenomenon of fluid flow lines in the trapezoidal model restores the actual flow characteristics of the near-well reservoir and enables the study of the microscopic sand production process and the mechanism of the near-well weakly-cemented sandstone reservoir. The trapezoidal models are mainly used in this experiment as particle migrations of the near-well reservoir are a more serious issue. The fluid flow line in the rectangular sandstone model advances gently, and the flow velocity distribution is more uniform, which is suitable for studying the sand production characteristics of far-well stratigraphy (Fig. 3b). There is a glass window above the sandstone model, allowing the direct observation of the change in the skeleton of the weakly-cemented sandstone and the microscopic process of sand production when the fluid flows through it. The maximum pressure of the thin section models is 15 MPa. In this work, the microscopic dynamic expansion patterns of sand production in thin section models were analyzed by photographic or video recording through the microscopic observation module.

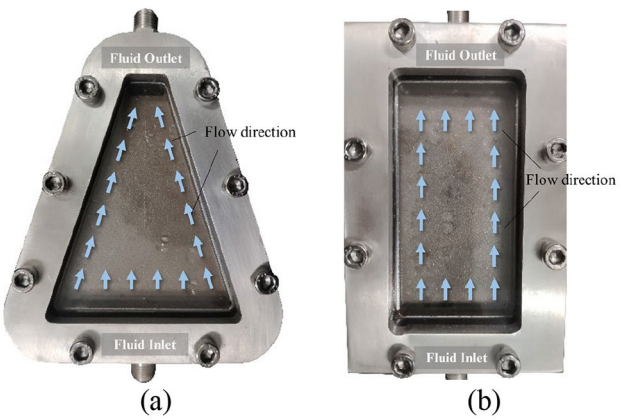

Fig. 3 The trapezoidal and rectangular sandstone models. **a** The trapezoidal simulation model and **b** the rectangular simulation model

Materials and conditions

The simulation sand sample was filled in the models to simulate the sanding stratigraphic units since thin section sandstone cores are hard to obtain. The simulation sand sample was configured with a median particle size of 160 μm and a uniformity factor of 7.3 using quartz sand. Epoxy resin was selected as the cementing agent for the experiment considering the production cost and the difficulty of adjusting the stratigraphic unit properties, which is also one of the commonly used cementing agents for making artificial cemented cores in the laboratory (Xu et al. 2017). Firstly, the simulation sand sample was mixed with the cementing agent in a certain proportion, after filling the model, placed a specified item on top to achieve the compaction and then dried at 80 °C for 3 h to produce weakly-cemented flake sandstone. Meanwhile, the standard cylindrical sandstones with the same composition and same cementing agent proportion were prepared to test uniaxial compressive strength (abbreviated as UCS), as shown in Fig. 4. The same overlay stress was applied to make the thin samples and the standard cylindrical samples as similar as possible, the same stress was applied, maintaining the same compaction before cementing. Hence, kept samples for the same mixing ratio have similar internal microstructure and strength values. The UCS of the standard cylindrical samples ranged from 0.02 to 1.33 MPa, which can be considered to be extremely weakly cemented (Fjær et al. 2021). This experiment calls

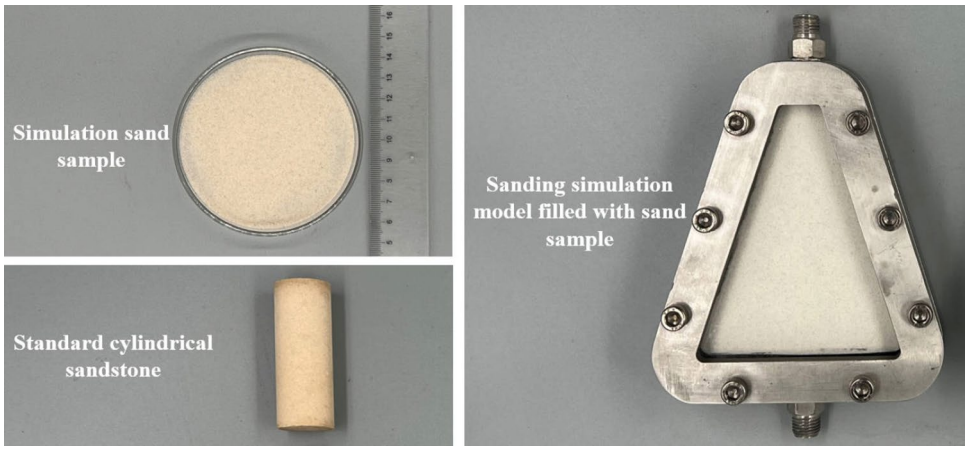

Fig. 4 View of simulation sand sample, standard cylindrical sandstone for UCS testing, and sand simulation model

for visual observation of the microscopic transport behavior of sand grains in the models, but crude oil's color causes visual interference, and functioning under a microscope is difficult. And the viscosity may cause clogging and holding pressure which may exceed the models' pressure resistance. Therefore, the experiments were conducted in freshwater to make sure both the microscope and the models could work properly, which is also one of the limitations of this research. The results of the sand production were subject to the composite effect of multiple factors such as displacement flow and fluid viscosity. This experiment was conducted at room temperature (25 °C), and a fluid flow rate of 125 mL/min was set constantly to minimize interference from the aforementioned parameters. The actual flow rate and pressure recorded by the sensors depend on the experimental displacement process and flow resistance. All experimental conditions are shown in Table 1.

Table 1 A summary table of all testing conditions

No.	Uniaxial compressive strength (MPa)	Model	Flow rate (mL/min)
1	0.202	Trapezoidal	125 ± 0.5
2	0.202	Rectangular	
3	0.703	Trapezoidal	
4	0.018	Trapezoidal	
5	0.029	Trapezoidal	
6	0.180	Trapezoidal	
7	0.166	Trapezoidal	
8	1.189	Trapezoidal	
9	0.382	Rectangular	
10	0.670	Trapezoidal	
11	0.674	Rectangular	
12	0.629	Trapezoidal	
13	1.019	Trapezoidal	
14	1.126	Trapezoidal	
15	1.334	Trapezoidal	

Method and procedure

After the sample preparation and cementation, the sanding simulation models are flushed with water injected from the liquid storage tank. The specific procedure of the experiment is as follows:

(a) Apply the trapezoidal or rectangular sanding models to the VSSA, ensuring that both upstream and downstream valves are kept open.
(b) Turn on the power of the video microscope and adjust the micro-magnification to focus on the simulated rock structure.
(c) Fill up the liquid storage tank and set the piston pump to the designed flow rate. Empty the sand collector and liquid collector, checking the connectivity and sealability.
(d) Turn on the data acquisition system and officially start the experiment.
(e) Observe and take pictures to record the sanding pattern in the models.
(f) End the experiment when the pressure reaches a relatively stable state.
(g) Export all data collection and take out the separated produced sand for drying and weighing.

During the experiment, freshwater from the liquid storage tank is pumped to the thin section model under pressure by the plunger pump, carrying out the sand grains inside it. Sand grains are transported to the sand collector module via pipes, and the waste liquid finally flows to the liquid collector after being separated from the sand. The experimental sandstone models are particularly small compared to the actual field scale, and the sand production reaches stability soon at the early stage. Each round of experiments lasts about 20 min.

Results and discussion

Wormhole sanding cavity

The wormhole sanding cavity found in the past studies was relatively simple, and this work fills the gap by discovering a more complex wormhole sanding cavity pattern. And for the first time, quantitative means are used to depict these sanding patterns and the underlying relationships between different strengths and wormholes. The main experimental results of complex sanding cavity patterns are studied in this part from qualitative description to quantitative analysis.

Sanding cavity of single-branch wormhole

Samples with different uniaxial compressive strengths are made through different ratios of the cementing agent. And some results of the single-branch wormhole (abbreviated as SBW) patterns in those samples are observed as shown in Fig. 5. SBW represents the sand production pore throat in the model that has only one branch or has more branches that are not interconnected. Most of the single-branch wormhole sanding cavities occur in models with 0.02 MPa–0.3 MPa UCS. The models in this strength range are usually extremely porous in structure and are highly susceptible to destabilization during fluid flow. Sand production reaches stability early in the experiment, and a stable sand production pattern can be observed within a short time after the fluid flow. The single-branch wormhole generally shows a large pore-throat pattern through the models (Fig. 5a–c). Figure 5d shows the rectangular sanding model of the experimental apparatus, and the experimental results also observe the wormhole sand production pattern. However, its cavity volume ratio is only 39.4% of that of the trapezoidal model at the same intensity, indicating that sand production will intensify under near-well confluence conditions, and the formation will face a more complex deficit pattern. The sanding cavity volume ratio reflects the volume of the wormhole sanding cavity to the sandstone model. With the increase in UCS, the sanding velocity of the weakly-cemented near-well reservoir gradually decreases, and the sanding cavity volume

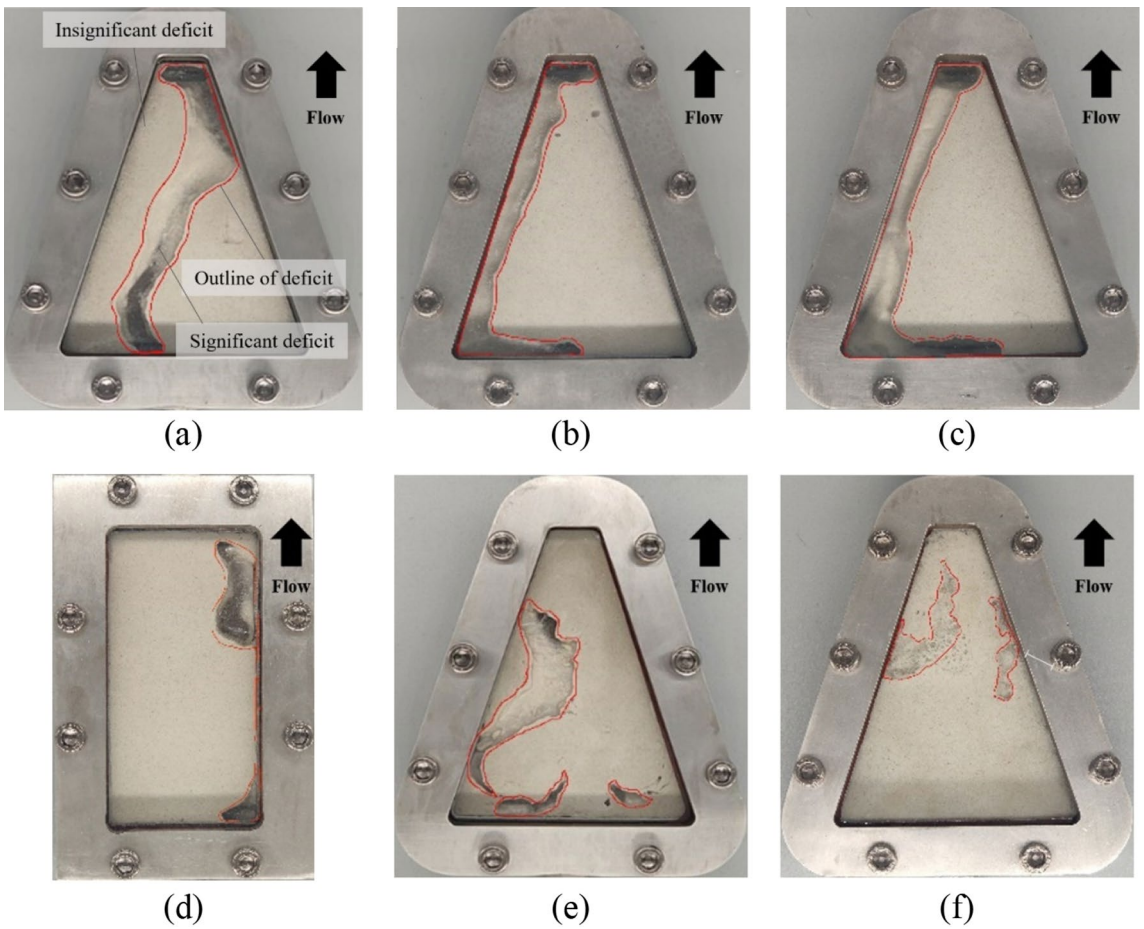

Fig. 5 Single-branch wormhole sanding cavity in different uniaxial compressive strength samples. **a** UCS of 0.018 MPa; **b** UCS of 0.029 MPa; **c** UCS of 0.202 MPa; **d** UCS of 0.202 MPa; **e** UCS of 0.703 MPa; and **f** UCS of 1.189 MPa

ratio decreases, while the extensional irregularity of the sand production deficit pattern becomes stronger, and the flow channel equivalent diameter and extension distance decrease significantly, as shown in Fig. 5e and f. The single-branch patterns may indicate that the near-well reservoirs are prone to rapid breakthroughs by fluid and the formation of large pore-throat high-permeability channels.

Sanding cavity of a multi-branch wormhole

The sanding cavity of a multi-branch wormhole (abbreviated as MBW) can be observed as more than one interconnected sand production deficit cavity, generally extending from a single-branch expansion. In the uniaxial compressive strength interval of about 0.02 MPa–1.33 MPa, 66.7% of the wormhole sanding cavity was observed to exhibit complicated multi-branch extension with one bifurcation or multiple bifurcations under the same flow conditions. Figure 6a and b shows the post-experimental deficit pattern of trapezoidal models with similar uniaxial compressive strengths, and MBW sanding pattern extends with two to four branches during the extension process, with each branch extending in different directions and velocities but basically along the flow direction. Figure 6c and d shows the sand production pattern of a wormhole sanding pattern observed in rectangular cores, with the number of branches ranging from 2 to 7, and the overall pattern is more irregular compared to trapezoidal models.

A quantitative description of the wormhole is beneficial to the subsequent study of the relationship between sand production patterns and reservoir flowability performance improvement. The denudation depth, equivalent diameter, extension length, and extension rate are proposed to quantify the sand production pattern of a wormhole. The denudation depth is the diameter of the sanding cavity in the vertical direction of the sample, and the equivalent diameter reflects the diameter in the horizontal direction. The combination of denudation depth and equivalent diameter reflects the overall wormhole scale. Since the wormhole shape is extremely irregular, the five largest points are measured and averaged to obtain the average maximum aperture for each wormhole. The average maximum aperture measurement results for each group are shown in Table 2. The extension length is measured directly, and it represents the extension degree of the wormhole cavity pattern in the fluid flow direction. The extension rate reflects how fast the extension length grows, calculated through the extension length and total flooding time. Because most of the MBW patterns are shallower than the SBW patterns in terms of denudation depth, with relatively smaller equivalent diameters, the average maximum apertures are, therefore, smaller as a result. And as shown in Table 2, the extension length of MBW is also relatively

Table 2 The average aperture for each wormhole

No.	Uniaxial compressive strength/MPa	Sanding cavity pattern	Average maximum aperture/mm	Extension length/mm
1	0.202	SBW	6.80	128.82
2	0.202	SBW	3.18	97.54
3	0.703	SBW	5.45	139.71
4	0.018	SBW	5.75	143.65
5	0.029	SBW	8.97	44.87
6	0.180	SBW	6.13	82.21
7	0.166	SBW	7.31	149.17
8	1.189	SBW	9.28	116.06
9	0.382	MBW	4.47	28.76
10	0.670	MBW	9.82	103.65
11	0.674	MBW	8.76	100.56
12	0.629	MBW	7.23	117.45
13	1.019	Others	0.31	197.52
14	1.126	Others	0.05	12.55
15	1.334	Others	0.80	158.65

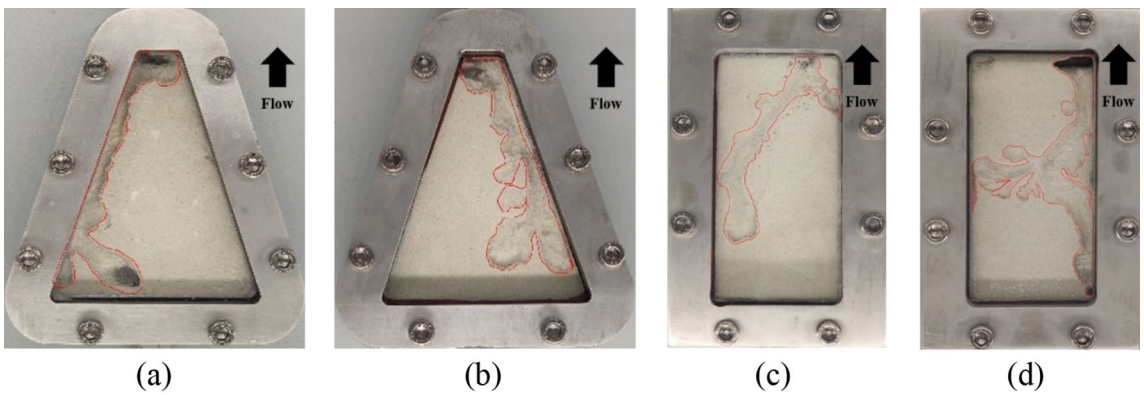

Fig. 6 Multi-branch wormhole sanding cavity in different uniaxial compressive strength samples. **a** UCS of 0.629 MPa; **b** UCS of 0.670 MPa; **c** UCS of 0.382 MPa; and **d** UCS of 0.674 MPa

smaller than SBW during the same flooding time, which indicates the slower extension rate of MBW. Thus, it can be concluded that the complex multi-branch pattern has the characteristics of simultaneous expansion of multiple branches, and a wide range of morphological extension, but a slow rate of reaching stable sand production. All of the wormhole patterns have a direct influence on the reservoir structure of the weakly-cemented sandstone.

A large number of wormhole sand production patterns were observed with the artificial simulation sandstone in different UCS, two-thirds of which were common single-branch patterns, while the others exhibited varied multi-branch extension patterns. The experimental final data are displayed in Fig. 7, which shows the sand production rate and patterns in different uniaxial compressive strengths. Since it is difficult to ensure absolute uniformity of tested samples and the UCS cannot accurately reflect the cementing strength of sanding models, the research only serves as a guide for the general law of strength influence rather than examining the specific impact on sand production patterns. Additionally, since the models were particularly small compared to the actual field scale, it is found that the final sand production patterns were slightly different between rectangular models and trapezoidal models for the same mixing ratio, which is also reflected in Fig. 7. Therefore, the sanding patterns are not discussed strictly in terms of trapezoidal and rectangular models. The strength is indeed a key factor affecting the quantity of sand produced from weakly-cemented sandstone formations and the sand production pattern of wormhole patterns. Due to the non-homogeneous cementation and random distribution of sand particles, the apparent pattern of weakly-cemented sandstones is complex and diversified, and the experimental results obtained from different classes of wormhole patterns lack obvious strength boundaries. Preliminary statistics show that there is a low occurrence of wormhole sanding patterns under the 0.75–1.5 MPa UCS, with an average sand production rate of 1.6 g and an average cavity volume ratio of 0.82%. Besides, the occurrence of MBW sanding pattern is 66.7% in the interval of 0.3–0.75 MPa, with an average sand production rate of 4.45 g, and an average cavity volume ratio of 8.55%. The models with UCS below 0.3 MPa showed mainly SBW sanding patterns with more produced sand, averaging 6.06 g, and a higher final cavity volume ratio averaging 12.52%. Preliminary statistical results show that with the increase in uniaxial compressive strength of samples, the single-branch wormhole sand production patterns in the models can be extended to multi-branch patterns.

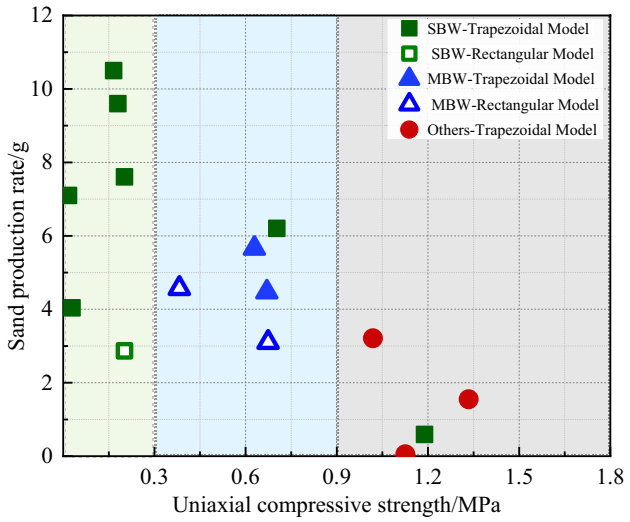

Fig. 7 Diagram of overall experimental results. Additional notes: As the UCS increased, other less wormhole-like sanding patterns appeared, which have been tentatively named "others," but they were not many and not the main point of this paper. The authors have counted them for the sake of rigor, which may become the priorities of future studies

Extending the performance of sanding wormhole

An obvious extension of the single-branch pattern (Fig. 8) has been observed under the condition of using the prepared sand sample configured with 0.6% cementing agent content, and the cemented sample's UCS was tested to be 0.202 MPa. At the outlet end, fluid first carries away unconsolidated loose sand to form an early fluid channel. The weakly-cemented sand exposed in the early fluid channel continues to be subjected to fluid forces, and the sand particle and weakly-cemented interface gradually flake off and begin to transport. The original bits of sand grains and sand masses replenish to the fluid channel, forming a larger flow space. The macroscopic performance of the simulated weakly-cemented sandstone is that a collapse deficit point first appears near the exit end at the early stage of the repulsion. The deficit point is continuously extended under the competition mechanism of sand exfoliation at the front, and the sand is continuously exited during the extension process. Meanwhile, the flow pressure difference between the models' inlet and outlet slowly decreases. When the pattern extends to the inlet side, a dominant large pore channel is produced in the simulation models and the flow pressure difference drops steeply, after which the sand production rate equilibrates and the pressure remains stable.

An expansion process of the more complex multi-branch extension sanding pattern is observed (Fig. 9) under the condition of using the prepared sand sample configured with 0.8% content of cementing agent, and the strength of the cemented sample was tested to be 0.674 MPa. Due to the limitation of the model's scale, the existing studies cannot avoid the influence of the boundary effect on the sand production pattern for the time being. The sanding patterns in

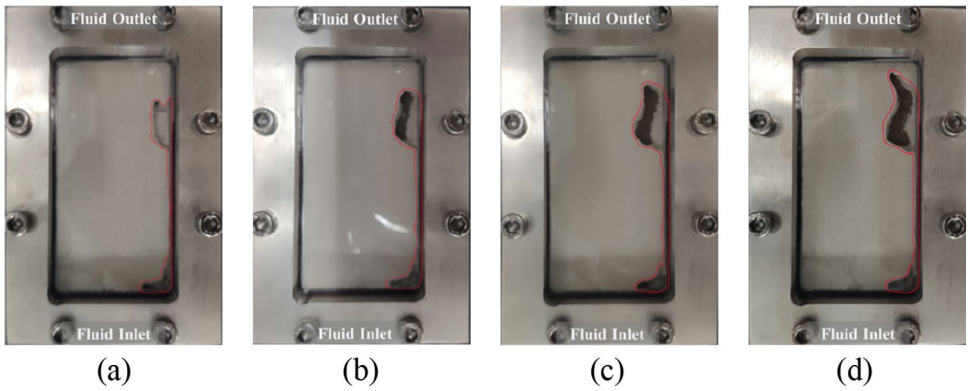

Fig. 8 The macroscopic extending performance of the sanding cavity of the single-branch wormhole. **a** The performance of the sanding cavity after the 30th second with total pressure drop 8.8 kPa; **b** the performance of the sanding cavity after the 180th second with total pressure drop 60.1 kPa; **c** the performance of the sanding cavity after the 420th second with total pressure drop 122.5 kPa; and **d** the performance of the sanding cavity after 1020th second with total pressure drop 195.5 kPa

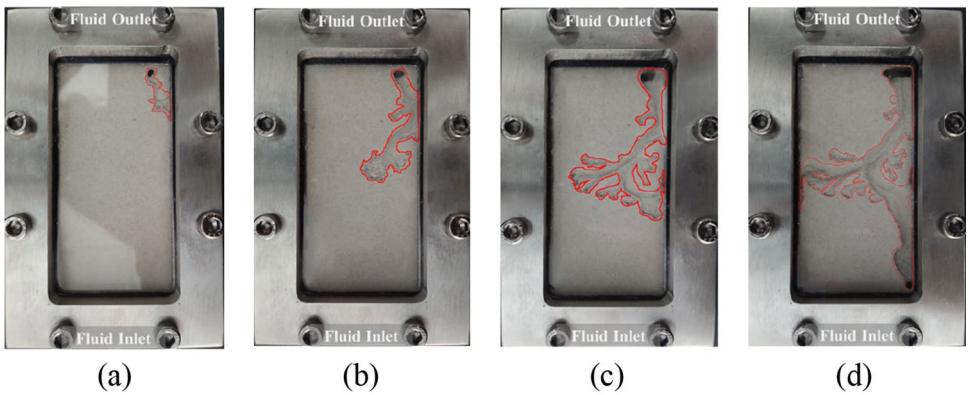

Fig. 9 The macroscopic extending performance of the sanding cavity of the multi-branch wormhole. **a** The performance of the sanding cavity after the 38th second with total pressure drop 11.6 kPa; **b** the performance of the sanding cavity after the 128th second with total pressure drop 65.0 kPa; **c** the performance of the sanding cavity after the 218th second with total pressure drop 185.3 kPa; and **d** the performance of the sanding cavity after 1118th second with total pressure drop 360.7 kPa

those samples tend to emerge along the edge face of the model when flushing, but the overall sand production patterns of the wormhole from different experimental results still reflect great variability. Comparing the differences between the above single-branch pattern and multi-branch pattern during dynamic extension, it is found that the monotonous single-branch wormhole can complete the longitudinal extension around the 180th second. In addition, the volume growth of the sanding pore mainly depends on the lateral expansion with no more branches generated, and the pore edge gradually expands outward under fluid flushing. The single-branch wormhole is observed at 1020th second as shown in Fig. 8d. The morphological scale is about twice that of the early stage. The longitudinal extension of the pore throat of the multi-branch wormhole is relatively slow, and the derived sub-pore throat has extension tendencies in all directions driven by the non-uniform flow field and the non-homogeneity of the model. The MBW sanding morphology is not strictly distinguished from the SBW sanding pattern, which might be considered an advanced form of the latter. It is highly possible that SBW is transformed to MBW after meeting the condition that is elaborated in the micro-mechanism below.

One important trend in this field from an experimental point of view is the scale upgrading of tests and the development of instruments for monitoring the morphology of sand production. The current indoor experiments on solid production simulation are still limited to small and medium scales which are much smaller than the actual oil reservoir conditions. As a result, it is restricted that investigating more realistic extension laws of sanding patterns and reservoir physical changes. In addition, the actual deficit of the sample and the physical alteration of the oil reservoir can only be grasped by accurately capturing and recording the sand

production patterns during the experiment. The sand prediction model can be advanced after more accurate knowledge of the generation mechanism of various sanding patterns and the relationship of their influence on the oil reservoir.

Flowability performance improvement

The following discussion focuses on the experimental results of the complex wormhole sand production morphology. This section presents a method to quantify the extent to which wormhole affects reservoir structure, providing an idea for applying experimental analysis results to actual oil fields. And this method requires first going through the pressure drop and sanding deficit volume situation in the wormhole mode.

In the process of displacement, the fluid will flush out the loose and weakly-cemented sand particles from the pore, reconstructing the sandstone skeleton, increasing the pore throat, and expanding the pore diameter. As the resistance to flow decreases, the sandstone is thus considered to change its flowability properties. The apparent phenomenon is that the deficit of the core and the extension of sand production patterns are gradually noticeable, while the pressure appears to be reduced to different degrees with the decrease in the flow resistance. The flow performance changes can be reflected in the pressure drop, sand production rate, and cavity volume ratio. It is found that there are large dynamic evolution differences under different sand production patterns by recording the experimental pressure difference and flow realities, with basically the same flow rate. The pressure of the water flooding process is divided into three stages: the transient high-pressure stage, the rapid pressure drop stage, and the stable low-pressure stage. The water flooding pressure of

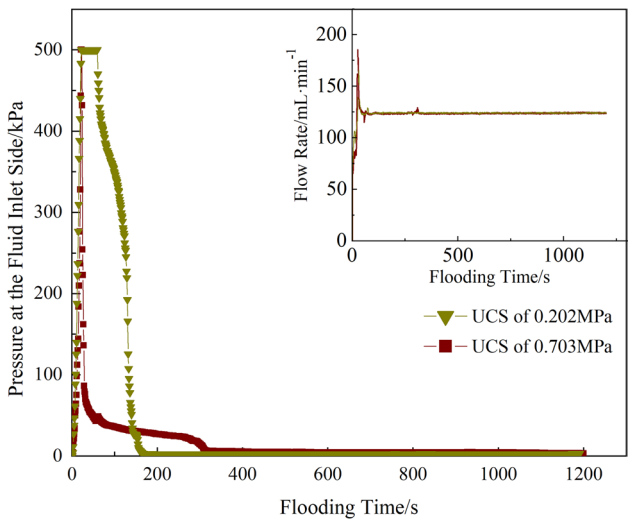

Fig. 10 Pressure at the fluid inlet side corresponding to the single-branch sand production patterns in trapezoidal models

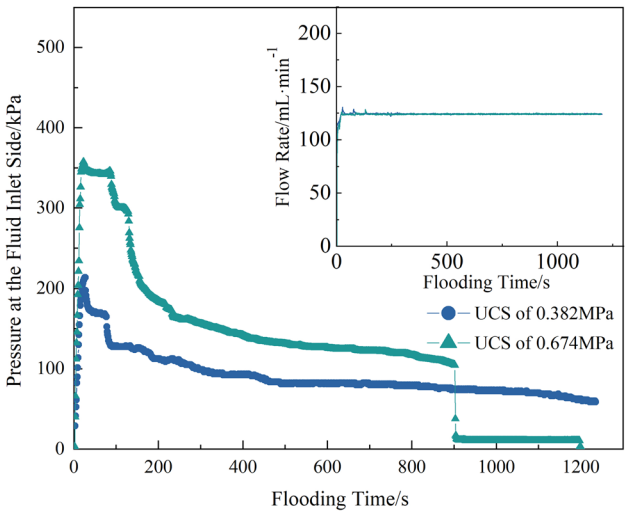

Fig. 11 Pressure at the fluid inlet side corresponding to the multi-branch sand production patterns in trapezoidal models

weakly-cemented sandstones peaks at the instant of pumping on, while the high-pressure phase in the wormhole sanding pattern lasts for a very short time, and the main differences are reflected in the pressure drop and low-pressure phases. The single-branch pattern mainly appears in extremely low-strength sandstone. The weak cementation surface is stripped rapidly, showing a rapid pressure drop curve, and the stable low pressure is reached within 200–300 s. The sand production is mainly concentrated in this period of pressure drop and nearly maintains the equilibrium if no other factors interfere in the low-pressure stage (Fig. 10). The complex multi-branch pattern is mainly found in higher strength sandstones. The duration of the pressure drop phase in this pattern is relatively longer, and the pressure drop from the peak is sluggish, which lasted about 810–1200 s in the experiment (Fig. 11) during which the sand particles produce continuously and steadily.

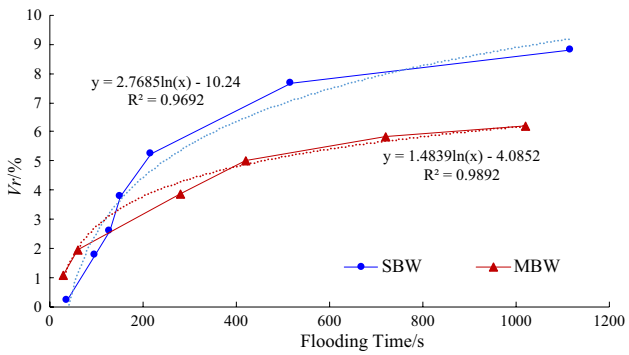

Fig. 12 Relationship between the cavity volume ratio and the water flooding time in wormhole sanding cavity

The slope of the sanding cavity volume–time curve in Fig. 12 can reflect the deficit rate of different sand production patterns. The single-branch wormhole pattern deficit is rapidly in the pressure drop stage, while the sand production cavity volume turns to a low-rate growth when it enters the low-pressure stage due to the delayed horizontal expansion of the deficit pore. The cavity volume growth rate of multi-branch wormhole sand production patterns in the pressure drop stage is lower than that of the single branch. In general, the sand production from the weakly-cemented sandstone behaves as follows: The sand grains are produced at a fast rate and in a large amount at the early stage, and then gradually decrease and stabilize in the later stage. The results show that the cavity volume ratio growth rate of the single-branch pattern is greater than that of the multi-branch pattern, which is also reflected in the sand production rate. In the way of single-branch extension, the cavity volume ratio gradually tends to a certain stable value after experiencing the transient violent sand grain migration and being able to form a large aperture, low tortuosity sand production channel that helps dredge the formation.

The formation of wormhole patterns increases the complexity of the pore-throat structure of sandstone reservoirs on the one hand and provides spatial conditions for the accumulation and circulation of oil on the other. In other words, when stable wormhole sanding cavity patterns are formed, this kind of sand production can produce a certain effect of unblocking the sandstone reservoir. A parameter is needed to directly reflect the relationship between different sand production patterns and the internal pore-throat structure of the rock and the flow performance of this kind of reservoir. Therefore, the study innovatively proposes the dredging efficiency and its calculation to characterize the improvement of the pore-throat structure and flow performance by sand grains migration during fluid flooding. The dredging efficiency of the wormhole sanding cavity pattern in the experiments can be quantified by pressure drop, cavity volume ratio, and average maximum aperture, as follows:

$$d_{\mathrm{ef}} = \sqrt[3]{\frac{\Delta p \cdot \overline{d}_{\max} \cdot V_{\mathrm{r}}}{T^3}}, \tag{1}$$

where d_{ef} is the dredging efficiency (MPa·mm/s), T is the water flooding time (s), ΔP is the pressure drop during water flooding (MPa), $\overline{d}_{\max}$ is the average maximum aperture (mm), and V_{r} is the sanding cavity volume ratio (%).

Figure 13 shows the results of cavity volume ratio and dredging efficiency for different experiments. The analysis of the above pressure drop curve and the law of cavity volume ratio show that different sand production patterns have different dredging efficiencies on reservoir formation. The single-branch pattern allows the fluid to quickly break through to form a single large channel, while the multi-branch extension mode allows multiple branches to expand simultaneously and prevents the fluid from quickly breaking through. The former is, therefore, more effective for sandstone dredging than the latter. The results of the above different experimental calculations yielded a range of 0.001270.00397 (MPa·mm s^{-1}) for the sand dredging efficiency of the single-branch pattern and a range of 0.0015–0.00278 (MPa·mm s^{-1}) for the multi-branch pattern. The average dredging efficiency of the two patterns is about 0.00263 (MPa·mm s^{-1}) and 0.00232 (MPa·mm s^{-1}), which means that the dredging efficiency of the SBW with macroporous structure is 1.13 times higher than that of the complex multi-branching wormhole pattern. This study concluded that the aperture of the main pore channel of the wormhole sand production pattern determines the dredging efficiency of the sand grains migration process to the weakly-cemented sandstone reservoir. In addition, the diverging effect in the MBW weakens the local high fluid speed area and micro-flow field effect, resulting in the slow extension of each branch and the consequent reduction of reservoir dredging efficiency. Therefore, the formation of a single-branch pattern in the weakly-cemented sandstones is more conducive to guaranteeing the reservoir flow performance later for oil. The active induction of single-branch wormhole pattern formation in large aperture flow channels with the technical assistance of proper sand release in the early stage may be of great importance for oilfield field enhancing production rate.

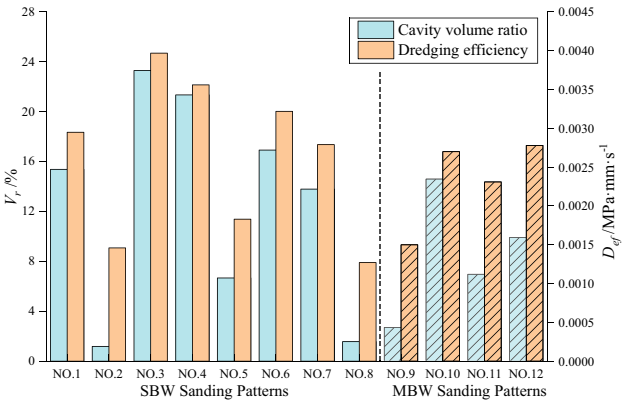

Fig. 13 Experimental results of cavity volume ratio and dredging efficiency of SBW and MBW sanding patterns

Micro-mechanism of sanding cavity extension

This section discusses the manner and process of sand detachment which was not clearly captured from a microscopic perspective in the previous studies. And the intrinsic relationship between complex wormhole sand production patterns and microscopic sand detachment behaviors is

revealed. Through this, this work proposes a new microscopic sanding mechanism of the wormhole extension and reveals the formation causes of complex multi-branching wormholes in non-homogeneous sandstones.

Sand competitive detachment mechanism

The local microfluidic field in the leading edge region of the wormhole throat is the main trigger for the forward extension of the wormhole pattern. The stratigraphic sand near the hole throat of the wormhole competes for stripping with single particles or clustered sand as the microscopic stripping unit. The detachment causes instantaneous changes in the skeletal structure of the leading edge of the wormhole cavity, resulting in subsequent changes in the microfluidic field therein. The formation of a local high fluid speed area at the detachment of the pore throat, intensifying the detachment of the nearby sand, and the leading edge of the pore throat of the wormhole is thus rapidly extending (Fig. 14). It is suggested that the sand competitive detachment mechanism is the root of particle transport under fluid–solid coupling, which is particularly prominent in weakly-cemented sandstones and present in all sand production modes. At very low compressive strengths, such as the 0.02–0.3 MPa strength interval samples in this study experiment, the cemented weak interface is preferentially decomposed into particles by the fluid rapidly before it is stripped in the repulsion. The single-branch forms in this experiment nearly reach the stable sanding stage within 50–300 s after water flux, and the extension distance remains stable, which is closely related to the sand competitive detachment mechanism. This mechanism explains why the sanding cavity of a single-branch wormhole appears and how it extends, but it does not yet explain the presence of a multi-branch wormhole. Therefore, the concurrent exfoliation mechanism is further revealed.

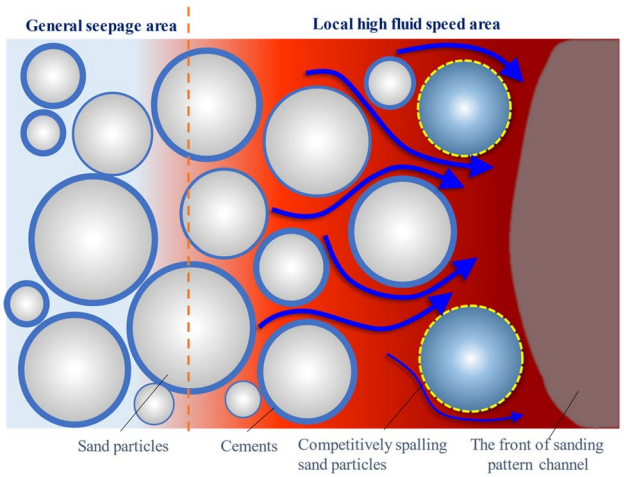

Fig. 14 Schematic diagram of the competitive sand detachment mechanism

Cavities concurrent extension mechanism

The non-homogeneity and higher cementation strength of the sandstone are the main causes of a single-branch wormhole extending to a multi-branch wormhole. With the increase in intergranular cementation strength, the stripping consumption time of the weakly-cemented surface is longer, and the overall stripping rate of the core decreases. Before the new weakly-cemented surface is completely stripped, the microfluidic field at the front of the wormhole channel acts on the frontier particles in all directions. Besides, due to the presence of non-homogeneity, multiple weakly-cemented surfaces may all meet the critical conditions for stripping and begin to flake off concurrently, thus forming multiple stripping surfaces, as shown in Fig. 15. When any branch penetrates the sand body to form a dominant flow channel, the fluid kinetic energy acting on other branches is weakened, and the extension stops or proceeds at a lower speed, thus forming a more stable multi-branched wormhole

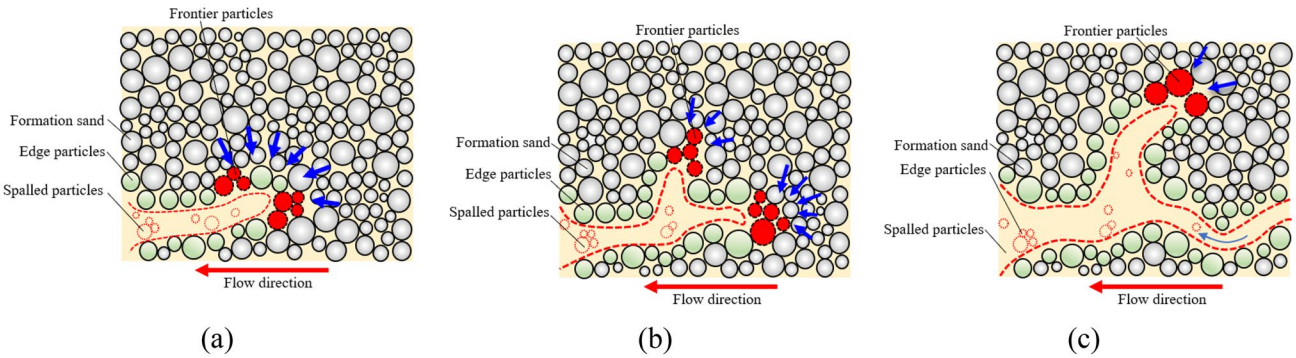

Fig. 15 Schematic diagram of the cavity concurrent extension mechanism of the MBW. **a** Concurrent detachment of weakly-cemented surfaces at the front of the wormhole pattern; **b** the branches of the wormhole extend forward; and **c** some branches extend quickly along the weakest cemented sand structure as dominant flow channels

pattern, which is summarized as cavities concurrent extension mechanism. This mechanism is also present in all samples which means that all samples can develop into multi-branches. However, the fluid force on sand is much greater than the detaching resistance in samples with too low cementation strength, and the detachment is too fast for other weakly-cemented frontier particles to move, thus hard to form multiple branches. But it cannot be denied that multi-branch wormholes can be observed in larger sample models. The single-branch wormholes and multi-branch wormholes discussed are only based on fixed-size models, while in fact, single-branch wormhole morphologies have the possibility of extending into multi-branching in the larger scale model. In that case, it is difficult to describe the sand production cavity patterns as "single" or "multiple," but qualitatively summarize them as simple wormhole sanding morphology with a small number of branches or complex wormhole sanding morphology with many branches. Based on the present experimental results, it is concluded that: When UCS is weaker than 0.3MPa, the reservoir sand production patterns tend to form simple wormhole patterns, and when UCS ranges between 0.3 and 0.9 MPa, they tend to form complex wormhole patterns.

This work provides a preliminary analysis of the critical conditions for sanding morphological extension by revealing the mechanism of sand detachment and wormhole expansion. Combining the particle critical stripping model (Dong et al. 2022) might lead to a desirable trend of sand production prediction and near-well reservoir numerical simulation. The near-well reservoir simulation technology is going to help engineers understand what the current structure is in the subsurface of old wells after a long period of sand production. Hence, it is beneficial to make a better production regime and to adjust the existing sand control and production enhancement methods.

Sand detachment forms

The above study revealed wormhole sanding cavity and extension mechanisms, and it was also found that two types of detachment form existed under both sand competitive detachment mechanism and cavities concurrent extension mechanism: discrete particle detachment and weakly-cemented interface detachment as shown in Figs. 16 and 17. The former is where sand particles are individually stripped from the core skeleton and carried away by fluids, while weakly-cemented interface detachment is the sand cluster stripped from the rock skeleton in the form of clumps and wrapped by fluid.

Discrete particle detachment is more common in weakly-cemented sandstone. When the fluid force on the particles is greater than the cementing force and friction between the particles, particles will be stripped from the rock skeleton

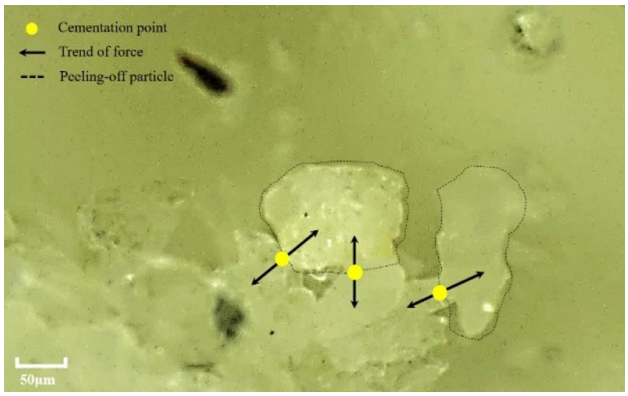

Fig. 16 The discrete particle detachment form near the fluid outlet side of the No.2 sample

Fig. 17 The weakly-cemented interface detachment form near the fluid outlet side of the No.8 sample

and carried away by the flooding fluid. The exfoliation of sand particles does not take place in isolation as solid particles meeting the above detachment conditions at the same time will compete to be exfoliated from the rock. However, due to the non-homogeneity, the rock fluid–solid interface of the sand will not be uniformly peeled off one by one, but along the direction of the worst solidification. The flow field is constantly changing, along with the centralized extending direction changing, resulting in a tortuous deficit channel (Fig. 18). Non-homogeneous particle cementation and particle accumulation are prevalent in weakly-cemented sandstone, causing differences in cementation strength between different interfaces and contact points between the particles. And these relatively weak bonding strength interfaces and contact points together form sand migration units of clusters that are easy to peel off from the rock. The microscopic stripping unit of the cluster in the form of weakly-cemented interface detachment is separated from the rock skeleton and transported out of its original position, causing an obvious deficit (Fig. 19).

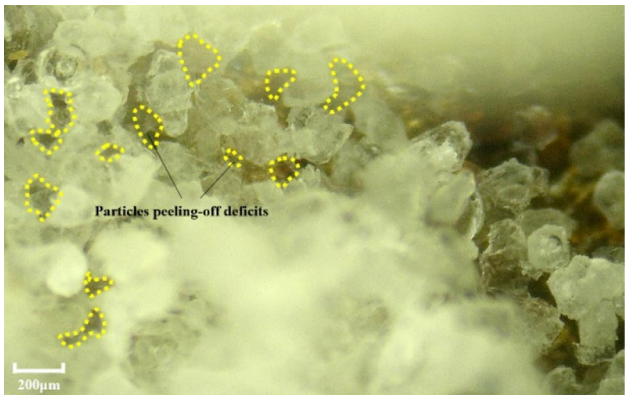

Fig. 18 Microscopic view of discrete particle detachment deficits in the middle of the No.2 sample

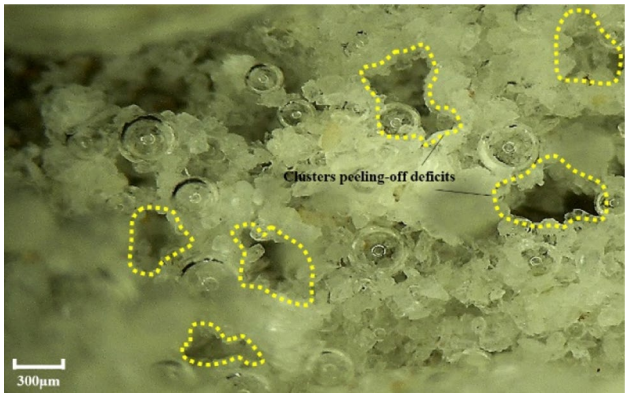

Fig. 19 Microscopic view of weakly-cemented interface detachment deficits in the middle of the No.8 sample

The microscopic mechanism of detachment in the form of weak cementation interfaces is the non-homogeneous cementation and non-homogeneous accumulation of sand particles. The cementation strength between particles inside the cluster sand is greater than the cementation strength of the weak cementation surface around it, and the fluid power flowing through is greater than the strength of this weak cementation surface, which triggers the gradual exfoliation of this sand cluster from the weak cementation surface. As shown in Fig. 20, in the pre-formed sand production orifice, the local microfluidic field acts on the sand skeleton in the adjacent orifice, and a weak cementation interface that is relatively easier to peel off appears, which is gradually peeled off under the action of the fluid. When this weak cementation interface is completely peeled off, the adjacent rock skeleton takes over to produce a new weak cementation interface. The flow field and the cementation strength of the adjacent skeleton reach equilibrium, forming a stable sand exfoliation pore channel.

Under the pre-designed flow condition and sanding simulation models with uniaxial compressive strength of 0.9–1.5 MPa, weakly-cemented interfaces can be observed to be stripped by the sand production simulation experiment, but it is difficult to capture the complete process of stripping due to the limitation of research conditions. The closer to the fluid convergence outlet, the higher the fluid pressure gradient, and the easier it is for the sand cluster to flake or further strip into particles. Therefore, a clear partial sand deficit can be observed at the outlet. The work finds that as the cementation strength of the sand increases, the harder it is for the cemented interface to meet the critical conditions, and the longer the peeling off consumption time. Hence, the pressure drop is relatively slower in the stronger cemented models, which is consistent with the reality that the stronger the cementation of the actual reservoir sandstone, the slower the production pressure reduction.

Conclusions

This paper discussed the macroscopic sand production patterns and the microscopic mechanism by conducting visual sanding simulation experiments. The main conclusions are as follows:

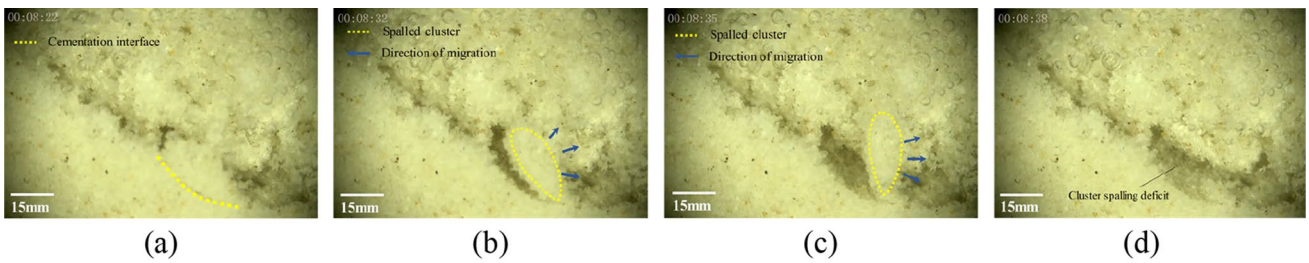

Fig. 20 Progress of the weakly-cemented interface detachment to form the microscopic deficit during the sanding simulation near the fluid outlet side of the No.11 sample. **a** It shows a weakly-cemented interface with detaching tendency; **b** the weakly-cemented interface started detaching; **c** the cluster sand produced from the weakly-cemented interface detaching started to be transported; and **d** formed a sand production cavity subsequently

1. It is found that the multi-branch wormhole sanding cavity can be extended from the single-branch pattern found in the previous research due to the non-homogeneity and randomness of cementation and construction in weakly-cemented sandstone. This reveals that the effect of sand production on the formation structure is complicated, and a more accurate portrayal of the reservoir deficit profile is needed if the variation law of sand-prone reservoir properties with production is to be predicted more precisely.
2. This paper proposes a quantitative way to depict these sanding patterns and the underlying relationships between different strengths and wormholes. The results show that with the increase in strength, the morphology of wormhole sand production tends to be complicated, and the aperture of sanding wormhole gradually decreases. The aperture of the single-branched wormhole, which generally occurs in very low-strength formations, is larger than the pore size of the multi-branched wormhole sand production pattern that occurs with increasing strength.
3. This work analyzes the improvement of flow performance of the overall models induced by the wormholes, and a quantitative method is established for evaluation. It is proposed that moderate pre-sanding actively induces the formation of a large cavity single-branch wormhole, which helps improve the near-well oil flowability of this kind of reservoir.
4. It reveals the forms of discrete sand particle detachment and weakly-cemented interface detachment during the expansion of the sanding patterns, the latter has exacerbated the sand production rate because of the large amount of sand migration. And it reveals the competitive detachment extension mechanism that induces sanding pattern expansion and the cavities concurrent extension mechanism that induces multi-branch patterns in non-homogeneous formation. These new microscopic discoveries and mechanisms can improve the understanding of macroscopic sanding phenomena and help in the subsequent research of reservoir deficit profile simulation.

Acknowledgements The first author would like to thank the China University of Petroleum (East China) for creating an enabling environment to conduct all the scientific research in the school.

Authors' contributions All authors contributed to the study's conception and design. Details of the contributions are as follows: YS and CD helped in conceptualization; YS worked in methodology; BZ and XZ contributed to validation; YS helped in formal analysis; YS, XZ, and GG helped in investigation; YS and CD helped in resources; BZ and XZ helped in data curation; YS and CD helped in writing—original draft preparation; YS and BZ helped in writing—review and editing; YS and GG helped in visualization; CD helped in supervision; and CD worked in funding acquisition. All authors read and approved the final manuscript.

Funding This research was financially supported by the National Natural Science Foundation of China (Grant No. 52074331).

References

Bagrezaie MA, Dabir B, Rashidi F (2022) A novel approach for pore-scale study of fines migration mechanism in porous media. J Petrol Sci Eng 216:110761. https://doi.org/10.1016/j.petrol.2022.110761

Dong C, Qiehai Y, Bo Z, Yubin W, Junyu D, Yang S, Lizhi W (2020) Visual experimental simulation on microscopic sand production morphologies and mechanisms in weakly consolidated reservoirs. Oil Dril Prod Technol 42(2):9. https://doi.org/10.13639/j.odpt.2020.02.017(inChinese)

Dong C, Zhou B, Huang F, Zhang L, Zhao Y, Song Y, Deng J (2022) Microscopic sand production simulation and visual sanding pattern description in weakly consolidated sandstone reservoirs. Pet Sci 19(1):279–295. https://doi.org/10.1016/j.petsci.2021.09.039

Du Z, Ma L, Wang X, Chen Z (2009) Study of sanding mechanism and a new model to calculate the sanding critical drawdown in loosened sandstone. In: Vol. All Days. SPE production and operations symposium. https://doi.org/10.2118/119588-MS

El-Sayed A-AH, Alsughayer AA (2001) A new concept to predict sand production from extended reach and horizontal wells. Paper presented at the SPE Middle East Oil Show. https://doi.org/10.2118/68134-MS

Fjær E, Holt RM, Horsrud P, Raaen AM, Risnes R (2021) Chapter 3—Geological aspects of petroleum related rock mechanics. In: Developments in petroleum science, vol 72. Elsevier, New York, pp 157–200

Gwamba G, Changyin D, Bo Z (2022) Investigating unary, binary and ternary interactive effects on pressure drawdown for optimal sand production prediction. J Petrol Sci Eng 218:111010. https://doi.org/10.1016/j.petrol.2022.111010

Habibi A, Ahmadi M, Pourafshary P, Ayatollahi S, Al-Wahaibi Y (2012) Reduction of fines migration by nanofluids injection: an experimental study. SPE J 18(02):309–318. https://doi.org/10.2118/144196-PA

Han G, Kwon T-H, Lee JY, Jung J (2020) Fines migration and pore clogging induced by single- and two-phase fluid flows in porous media: from the perspectives of particle detachment and particle-level forces. Geomech Energy Environ 23:100131. https://doi.org/10.1016/j.gete.2019.100131

Hashemi A, Borazjani S, Dang-Le B, Yin Loi G, Nguyen Cao C, Badalyan A, Bedrikovetsky P (2022) Formation damage by fines breakage and migration. Paper presented at the SPE international conference and exhibition on formation damage control. https://doi.org/10.2118/208810-MS

Jin Y, Li Y, Wu N, Yang D (2021) Characterization of sand production for clayey-silt sediments conditioned to openhole gravel-packing:

experimental observations. SPE J 26(06):3591–3608. https://doi.org/10.2118/206708-PA

Ju B, Dai S, Fan T, Wu H, Li S, Zhang M (2006) A novel 3D field-scale reservoir numerical simulator for predicting the fines migration and production performance. Paper presented at the SPE Europec/EAGE annual conference and exhibition. https://doi.org/10.2118/99797-MS

Khilar KC, Fogler HS (1983) Water sensitivity of sandstones. Soc Petrol Eng J 23(01):55–64. https://doi.org/10.2118/10103-PA

Morita N (1994) Field and laboratory verification of sand-production prediction models. SPE Drill Complet 9(04):227–235. https://doi.org/10.2118/27341-PA

Nouri A, Vaziri H, Belhaj H, Islam R (2003) Comprehensive transient modeling of sand production in horizontal wellbores. Paper presented at the SPE Annual Technical Conference and Exhibition. https://doi.org/10.2118/84500-MS

Nouri A, Vaziri H, Belhaj H, Islam MR (2007) Comprehensive transient modeling of sand production in horizontal wellbores. SPE J 12(04):468–474. https://doi.org/10.2118/84500-PA

Nouri A, Kuru E, Vaziri H (2009) Elastoplastic modelling of sand production using fracture energy regularization method. J Can Pet Technol 48(04):64–71. https://doi.org/10.2118/09-04-64

Polillo A, Vassilellis GD, Graves RM, Crafton JW (1994) Simulation of sand arching mechanics using an elasto-plastic finite element formulation. SPE Adv Technol Ser 2(01):76–85. https://doi.org/10.2118/23728-PA

Prempeh K, Chequer L, Badalyan A, Bedrikovetsky P (2020) Effects of kaolinite on fines migration and formation damage. Paper presented at the SPE international conference and exhibition on formation damage control. https://doi.org/10.2118/199293-MS

Russell T, Pham D, Neishaboor MT, Badalyan A, Behr A, Genolet L, Kowollik P, Zeinijahromi A, Bedrikovetsky P (2017) Effects of kaolinite in rocks on fines migration. J Nat Gas Sci Eng 45:243–255. https://doi.org/10.1016/j.jngse.2017.05.020

van den Hoek PJ, Hertogh GMM, Kooijman AP, de Bree P, Kenter CJ, Papamichos E (2000) A new concept of sand production prediction: theory and laboratory experiments. SPE Drill Complet 15(04):261–273. https://doi.org/10.2118/65756-PA

Volonté G, Scarfato F, Brignoli M (2013) Sand prediction: a practical finite-element 3D approach for real field applications. SPE Prod Oper 28(01):95–108. https://doi.org/10.2118/134464-PA

Wan RG, Wang J (2004) Analysis of sand production in unconsolidated oil sand using a coupled erosional-stress-deformation model. J Can Petrol Technol. https://doi.org/10.2118/04-02-04

Wang H, Sharma MM (2018) The role of elasto-plasticity in cavity shape and sand production in oil and gas wells. SPE J 24(02):744–756. https://doi.org/10.2118/187225-PA

Wang Y, Zhang B (2002) A laboratory research for the sand-production mechanism of viscous oil reservoirs in Fula oil field. Pet Explor Dev 29(4):2. https://doi.org/10.3321/j.issn:1000-0747.2002.04.035(inChinese)

Wei Y, Wang A, Dong C, Liu C (2011) Prediction model for critical sanding pressure drawdown in horizontal wells based on characteristic break radius. J China Univ Petrol (ed Nat Sci) 35(2):6. https://doi.org/10.3969/j.issn.1673-5005.2011.02.015. (**in Chinese**)

Weingarten JS, Perkins TK (1995) Prediction of sand production in gas wells: methods and gulf of mexico case studies. J Petrol Technol 47(07):596–600. https://doi.org/10.2118/24797-PA

Xu H, Xiong Y, Wang Y, Zhou W, Wang L, Jiang Q (2017) Preparation and evaluation on artificial core of extra high permeability unconsolidated sandstone. Oil Drill Prod Technol 39(04):477–483. https://doi.org/10.13639/j.odpt.2017.04.015. (**in Chinese**)

You Q, Lu X, Luan Z (2004) Particle migration in loose sandstone reservoirs. Pet Explor Dev 31(6):5. https://doi.org/10.3321/j.issn:1000-0747.2004.06.028. (**in Chinese**)

You Z, Badalyan A, Bedrikovetsky P, Hand M, Jenson D (2013) Productivity decline due to fines migration (modelling and field case). Paper presented at the International Petroleum Technology Conference. https://doi.org/10.2523/IPTC-17059-MS

Zeng X, He G, Sun F, Wang S (2005) Influences of sand production on permeability and experiments on sand production characters in SZ36-1 oil field. Pet Explor Dev 32(6):4. https://doi.org/10.3321/j.issn:1000-0747.2005.06.026(inChinese)